Electronic Supplementary Information (ESI) for

Band gap engineered, oxygen-rich TiO_2 for visible light induced photocatalytic reduction of CO_2

Lling-Lling Tan,[a] Wee-Jun Ong,[a] Siang-Piao Chai*[a] and Abdul Rahman Mohamed[b]

[a]Low Carbon Economy (LCE) Group, Chemical Engineering Discipline, School of Engineering, Monash University, Jalan Lagoon Selatan, 46150 Bandar Sunway, Selangor, Malaysia.

[b]Low Carbon Economy (LCE) Group, School of Chemical Engineering, Universiti Sains Malaysia, Engineering Campus, Seri Ampangan, 143000 Nibong Tebal, Pulau Pinang, Malaysia.

*Corresponding author:

Tel: +603-5514 6234; Fax: +603-5514 6207

E-mail address: chai.siang.piao@monash.edu

(1) Detailed experimental procedures

Chemicals. All chemicals were of analytical reagent-grade and deionized water was used throughout the experiment. Titanium (IV) butoxide (TBT), $C_{16}H_{36}O_4Ti$ (Sigma Aldrich Malaysia, > 97.0% purity) was used as the titania precursor. Hydrogen peroxide, H_2O_2 (R&M Chemicals, 30%) was used as the chemical modifier. Pure anatase TiO_2 nanopowder (Sigma Aldrich Malaysia, > 98.0%) and Degussa P25 were used as the control semiconductor photocatalysts. All chemicals were used as received without any further purification.

Synthesis of O_2-TiO_2. In a typical synthesis, TBT (5.5 mL) was added into 150 mL of cold water (5 ^oC) to form hydrolyzed titanium species. The precipitate obtained was repeatedly washed with water and stirred with H_2O_2 (80 mL) for 1 h to form a peroxo-titanate complex. The solution, on heating at 50 ^oC for 3 h underwent gelation, which was then dried in an air oven at 100 ^oC for 24 h. The yellowish solid material obtained was then subjected to calcination at 400 ^oC for 2 h at a heating rate of 10 ^oC/min, before characterization.

Characterization techniques. The surface morphology and chemical composition of the as-synthesized O_2-TiO_2 sample were analyzed by a field emission scanning electron microscopy (FESEM) (Hitachi SU8010) equipped with an Oxford-Horiba Inca XMax50 energy dispersive X-ray (EDX). High resolution transmission electron microscopy (HRTEM) images were taken with a JEOL JEM-2100F microscope operating at 200 kV. The TEM sample was prepared by depositing a drop of diluted suspension in ethanol on a lacey-film-coated copper grid. Raman spectra were recorded at room temperature on a Renishaw inVia Raman Microscope in the back-scattering geometry with Ar^+ laser excitation at 514 nm in the range of 100-3000 cm^{-1}. The X-Ray powder diffraction (XRD) data were obtained on a Bruker AXS D8 Advance X-Ray diffractometer with Cu Kα radiation (λ = 0.15406 nm) at a scan rate (2θ) of 0.02^o s^{-1}. The accelerating voltage and applied current were 40 kV and 40 mA,

respectively. The lattice parameters of anatase TiO_2 *a* and *c* were calculated from (101) and (200) reflections of the XRD pattern using Eq. 1, where *h, k, l* are the miller indices and d is the interplanar spacing calculated from the 2θ angle using the Bragg's Law (Eq. 2). The amount of rutile phase in O_2-TiO_2 and P25 were calculated using Spurr Equation (Eq. 3), where F_R is the amount of rutile in an anatase-rutile mixture, I_A (101) and I_R (110) are the anatase and rutile main peak intensities, respectively.

$$\frac{1}{d^2} = \frac{h^2 + k^2}{a^2} + \frac{l^2}{c^2} \quad (1)$$

$$d = \frac{\lambda}{2\sin\theta} \quad (2)$$

$$F_R = \frac{1}{1+0.8[I_A(101)/I_R(110)]} \quad (3)$$

The X-ray photoelectron spectroscopy (XPS) wide and narrow scan spectra were acquired using AXIS Ultra DLD, Kratos, equipped with an Al Kα X-ray source (1486.6 eV) at 10 mA, 15 kV, analyzing 300 µmm x 700 µmm area under 3.1 x 10^{-9} torr ultra vacuum environment. The spectra were analyzed using vision software which included vision manager and vision processing. All spectra were charge corrected by means of adventitious carbon signal (C 1s) at 284.6 eV. The linear method was used for background subtraction and curve fitting. Ultraviolet-visible (UV-Vis) absorbance spectra were obtained using a UV-Vis spectrophotometer (Agilent, Cary 100) equipped with an integrated sphere. The absorbance spectra of the photocatalysts were analyzed under ambient temperature in the wavelength ranging from 300-800 nm. The band gap energies of the photocatalysts were determined from the Kubelka-Munk function, F(R) and the extrapolation of Tauc plot which is a plot of $[F(R).hv]^{1/2}$ versus *hv*. A Nicolet iS10 FTIR spectrometer was used for recording the FTIR spectra of the H_2O_2-modified (oxygen-rich) and control TiO_2 intermediate.

Photocatalytic CO_2 reduction experiment. The photocatalytic experiment for the reduction of CO_2 was conducted at ambient condition in a homemade, continuous gas flow reactor. Highly pure CO_2 (99.999%) was bubbled through water (sacrificial reagent) to produce a mixture of CO_2 and water vapor into the photoreactor at atmospheric pressure. The flow rate of CO_2 was fixed at 5 ml/min. Prior to irradiation, CO_2 was purged through the quartz tube loaded with coated photocatalysts (O_2-TiO_2, $ATiO_2$) on glass rods for 30 min to remove any excess air and to ensure complete adsorption of gas molecules. The visible light source was then turned on to initiate the photocatalytic reaction. The reactant gas was in contact with the photocatalyst under the illumination of 15-W energy-saving daylight bulbs (8.6 mW/cm^2) to provide a full spectrum emission without any filter to simulate the sunlight source. The experimental set-up is illustrated in Fig. S1. The generated gases were collected at 1 h intervals and were analyzed by an Agilent 7890A gas chromatograph (GC), equipped with a flame ionization detector (FID). The CH_4 product yield was calculated using Eq. 4. Control experiments were conducted under N_2/H_2O flow as well as in dark condition (without irradiation of light source) to ensure that the CH_4 product formed was due to the photoreduction of CO_2.

$$\text{Yield}\left(\mu\text{mol CH}_4\ g_{cat}^{-1}\ h^{-1}\right) = \frac{(C_{final,CH_4} - C_{initial,CH_4}) \text{ x volumetric flow rate of product gas}}{\text{mass of photocatalysts used}} \quad (4)$$

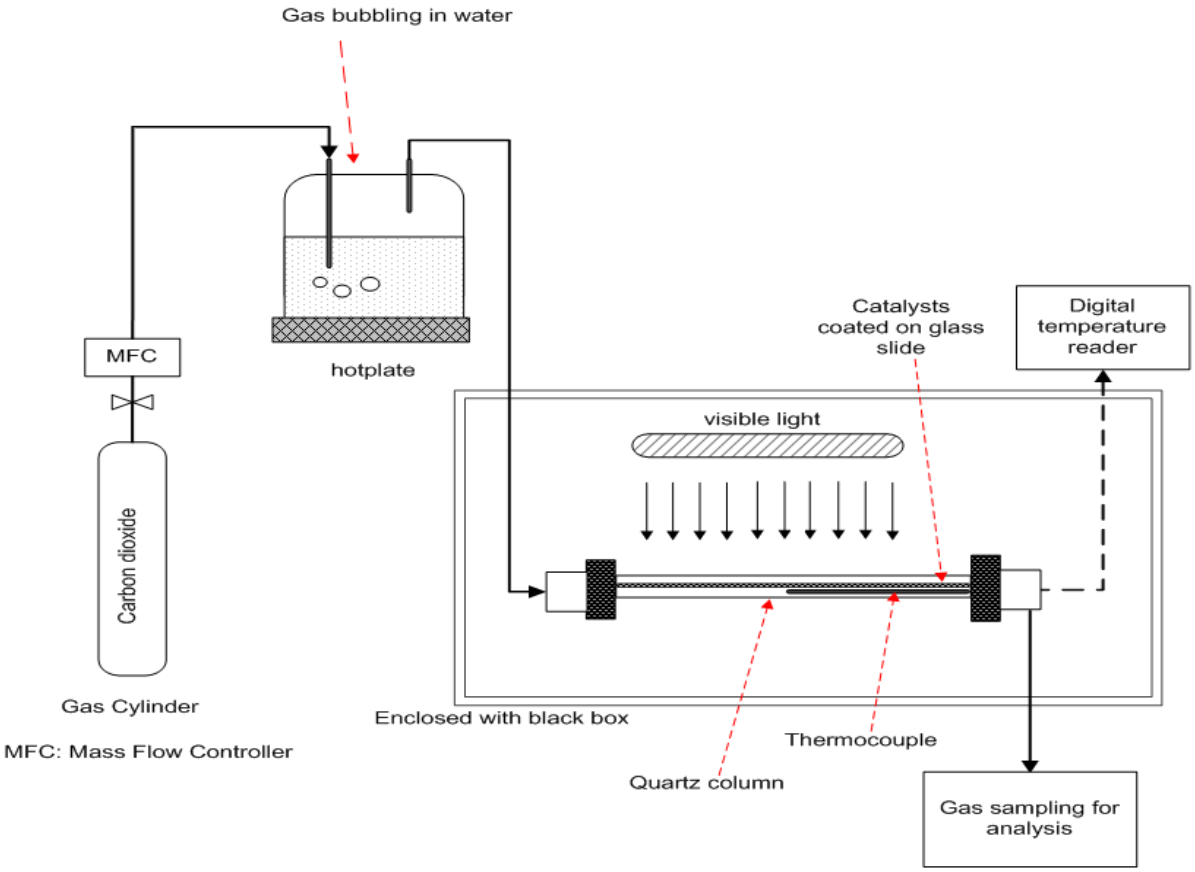

Fig. S1 Experimental set-up for the photocatalytic reduction of CO_2 under visible light irradiation

(2) Control experiments

Additional experiments were performed to verify that the band gap narrowing and photocatalytic enhancement of O_2-TiO_2 were due to the presence of oxygen excess defects. Using XRD patterns (Fig. S2) and the Spurr Equation (Eq. 3), the fraction of rutile phase, F_R present in O_2-TiO_2 (F_R = 0.356) was found to be close to that of the commercial Degussa P25 (F_R = 0.350). UV-Vis characterizations were then repeated for both P25 and pure rutile TiO_2, and were compared with O_2-TiO_2. From Fig. S3A, O_2-TiO_2 showed an obvious red shift at the absorption edge, indicating a narrowing of band gap, which was confirmed using a Tauc plot of the modified Kubelka-Munk (KM) function (Fig. S3B). O_2-TiO_2 exhibited the lowest band gap of 2.95 eV, while P25, $ATiO_2$ and pure rutile had estimated band gaps of 3.25, 3.20 and 3.00 eV, respectively.

In addition, the photocatalytic reduction of CO_2 was also repeated using the commercial P25 photocatalyst (see Fig. 4 in manuscript). It was observed that P25 exhibited low photoactivity towards the conversion of CO_2 under visible light. The O_2-TiO_2 sample showed an enhancement factor of 5.2 over P25. As the fraction of rutile phase in O_2-TiO_2 was close to that of P25, we can confirm that the band gap narrowing and photocatalytic enhancement were attributed to the oxygen-rich nature of our final product.

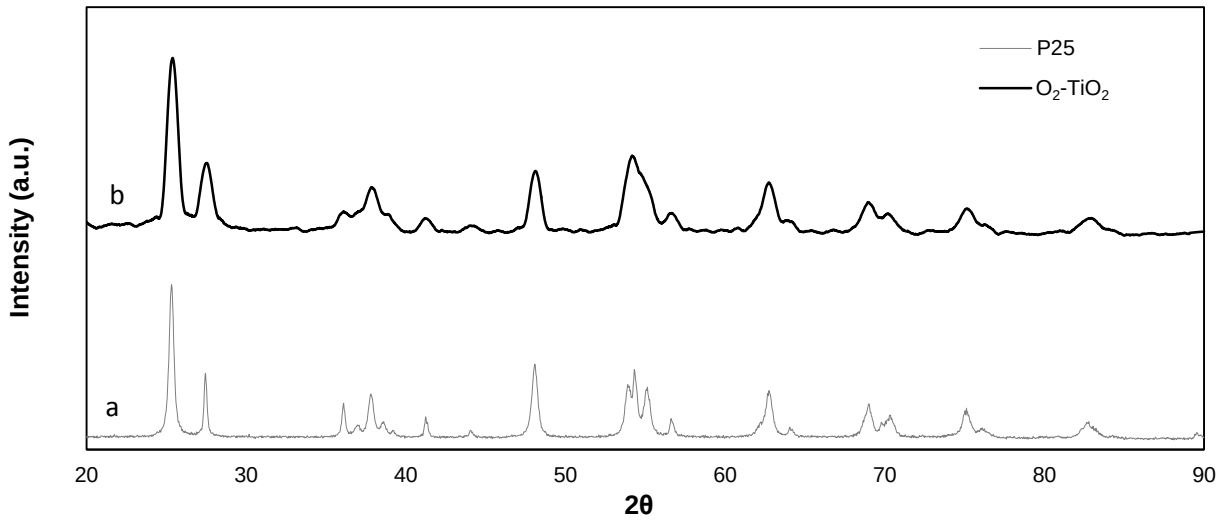

Fig. S2 XRD patterns of (a) P25 and (b) O_2-TiO_2 photocatalysts.

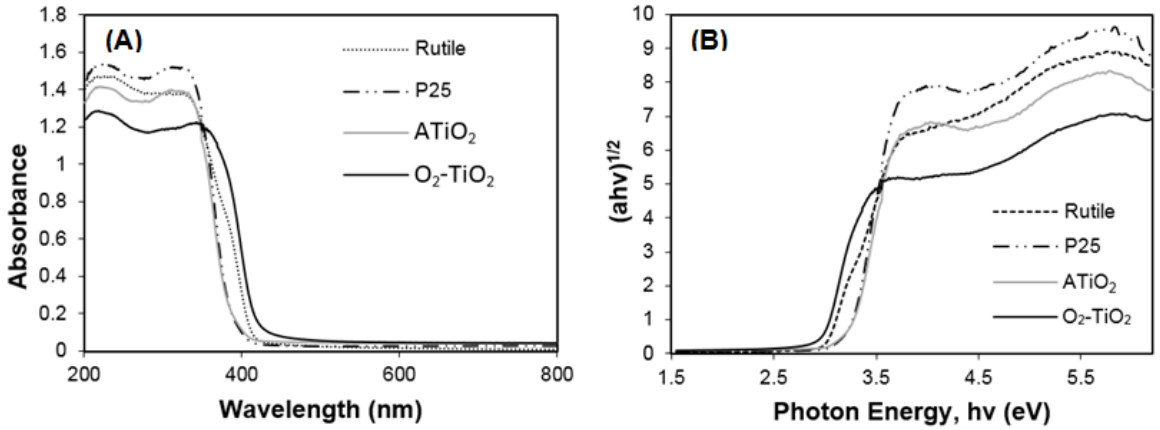

Fig. S3 (A) UV-Vis DRS and (B) plot of the transformed KM function for rutile, P25, $ATiO_2$ and O_2-TiO_2.

(3) FTIR spectra of the peroxo-titanate complex

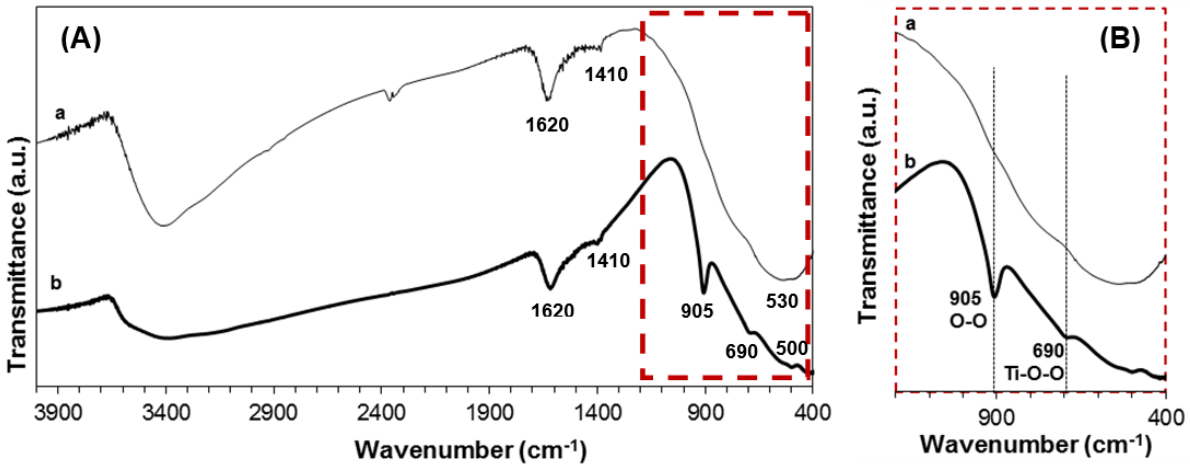

Fig. S4 (A) FTIR spectrum of 100 ^{o}C dried TiO_2 precursor: (a) control and (b) H_2O_2-modified TiO_2 intermediate, (B) Enlarged spectra for wavenumber range 400-1200 cm^{-1}.

(4) TEM and HRTEM images of $ATiO_2$

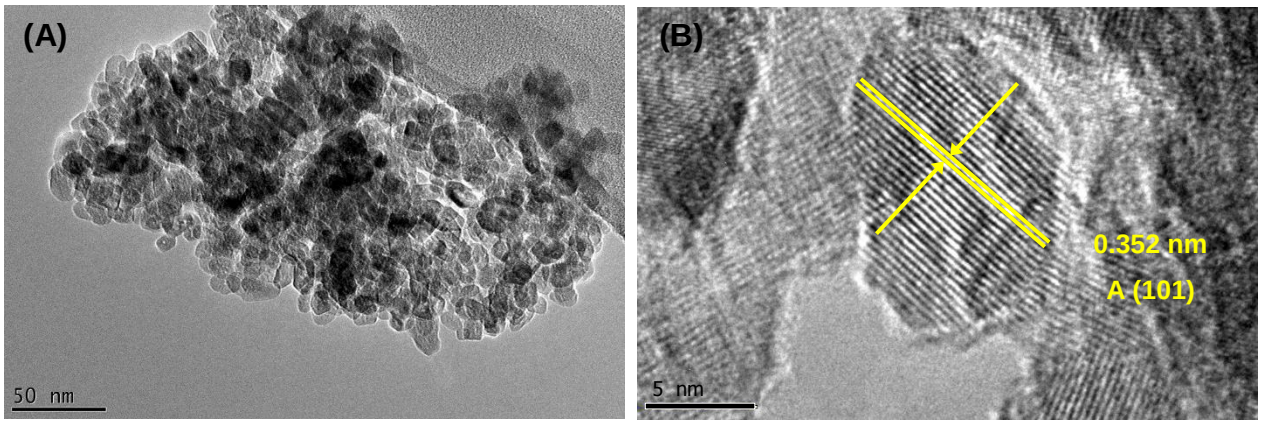

Fig. S5 (A) TEM and (B) HRTEM images of $ATiO_2$.

(5) Atomic structures of $ATiO_2$ and $(O_2)_O$

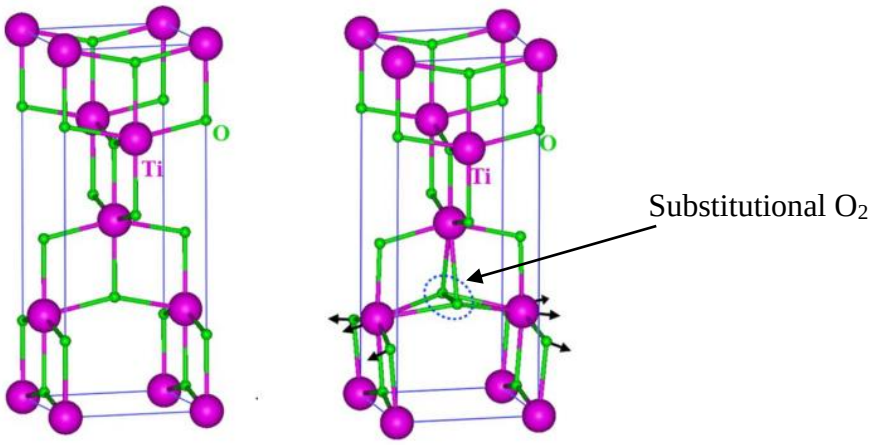

Fig. S6 Atomic structures of (A) $ATiO_2$ and (B) $(O_2)_O$.[1]

(6) Light spectrum of daylight bulb used in photocatalytic experiments

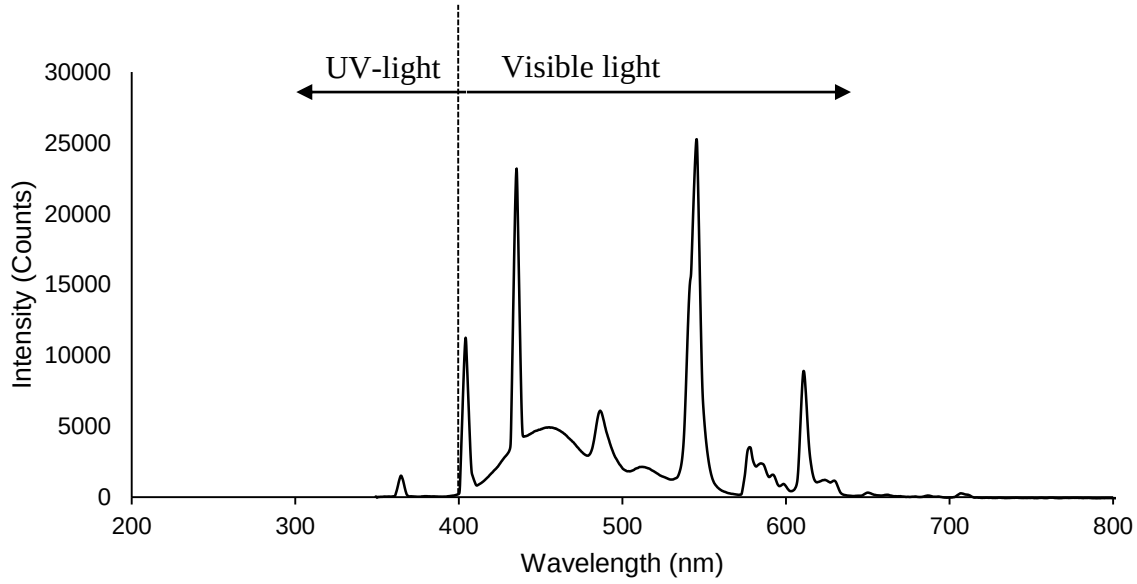

Fig. S7 Light spectrum of the daylight bulb used in the photoreduction of CO_2.

(7) Reaction mechanism for the photocatalytic reduction of CO_2 over O_2-TiO_2

As discussed in the manuscript, the two primary factors responsible for the high visible light photoactivity of O_2-TiO_2 are (i) the band gap narrowing effect of the oxygen excess defect and (ii) the enhanced absorption intensity in the visible region. The reaction mechanism over TiO_2 photocatalyst has been studied in our previous reports.[2,3,4] The photocatalytic conversion of CO_2 to CH_4 over the O_2-TiO_2 photocatalyst can be understood using the energy band theory, which is based on the relative positions of the conduction band (CB), valence band (VB), and redox potentials. The overall mechanism of the CO_2 transformation process is a sequential combination of H_2O oxidation and CO_2 reduction. In general, photo-excited electrons can be consumed effectively, if the reduction potential of the reaction is lower than the CB potential of the semiconductor. The CB flatband potential of O_2-TiO_2 (−0.5 V vs. normal hydrogen electrode (NHE), pH = 7)[5] is more negative than the reduction potential of CO_2/CH_4 (−0.24 V vs. NHE, pH = 7).[6] This indicates that the photogenerated electrons and holes on the irradiated O_2-TiO_2 can react with adsorbed CO_2 and H_2O to produce CH_4 via an eight-electron reaction (see Fig. S8). The major reaction steps in the photocatalytic CO_2 reduction process can be summarized by Eq. 5-7.

$$TiO_2 \xrightarrow{hv} e^-_{CB}(TiO_2) + h^+_{vb}(TiO_2) \qquad (5)$$

$$TiO_2\left(2h^+_{VB}\right) + H_2O \rightarrow 2H^+ + \frac{1}{2}O_2 \qquad [E^o = +0.82\ V] \qquad (6)$$

$$CO_2 + 8H^+ + 8e^- \rightarrow CH_4 + 2H_2O \qquad [E^o = -0.24\ V] \qquad (7)$$

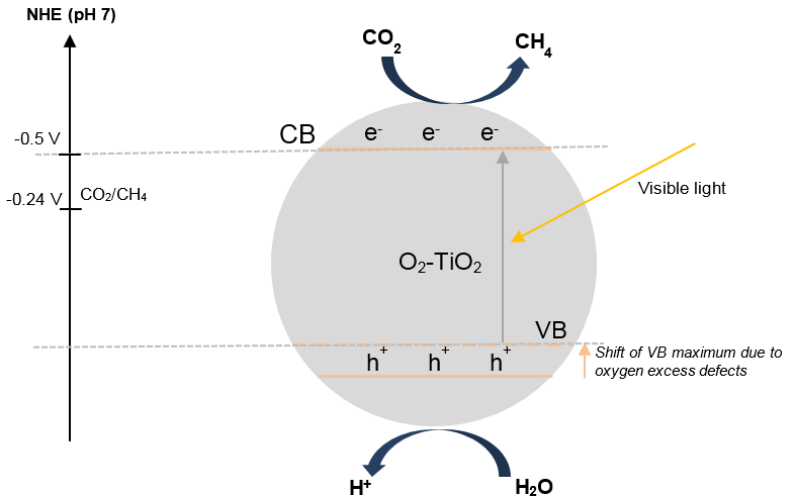

Fig. S8 The schematic of visible absorption and photocatalytic mechanism in the presence of O_2-TiO_2 nanoparticles.

References

1 S. Na-Phattalung, M. F. Smith, K. Kim, M.-H. Du, S.-H. Wei, S. B. Zhang and S. Limpijumnong, *Phys. Rev. B*, 2006, **73**, 125205.

2 M. M. Gui, S.-P. Chai, B.-Q. Xu and A. R. Mohamed, *Sol. Energy Mater. Sol. Cells*, 2014, **122**, 183.

3 W.-J. Ong, M. M. Gui, S.-P. Chai and A. R. Mohamed, *RSC Adv.*, 2013, **3**, 4505.

4 L.-L. Tan, W.-J. Ong, S.-P. Chai and A. R. Mohamed, *Nanoscale Res. Lett.*, 2013, **8**, 465.

5 Y. Li, W.-N. Wang, Z. Zhan, M.-H. Woo, C.-Y. Wu and P. Biswas, *Appl. Catal., B*, 2010, **100**, 386.

6 N. Zhang, S. Ouyang, T. Kako and J. Ye, *Chem. Commun.*, 2012, **48**, 1269.